



Contents lists available at ScienceDirect

Microelectronics Journal

journal homepage: www.elsevier.com/locate/mejo

Super-regenerative receiver at 433 MHz

João Paulo Carmo*, José Carlos Ribeiro, Paulo Mateus Mendes, José Higinio Correia

University of Minho, Dept. Industrial Electronics, Campus Azurém, 4800-058, Guimarães, Portugal

ARTICLE INFO

Article history:
Received 30 June 2010
Received in revised form
14 February 2011
Accepted 16 February 2011
Available online 9 March 2011

Keywords:
Super-regeneration
RF receiver
Super-regenerative receiver
CMOS

ABSTRACT

This paper presents a receiver for operation in the 433 MHz ISM band. The selected architecture explores the super-regeneration phenomena to achieve a high sensitivity for applying in wireless implantable microsystems. This radio-frequency (RF) chip can be supplied with a voltage of only 3 V for demodulating signals with powers in the range (−100, −40) dB. The codulation (modulation and coding) scheme of the binary data is a variation of the Manchester code combined with on/off keying (OOK) modulation. The AMIS 0.7 μm CMOS process was selected for targeting the requirement to fabricate a low-cost receiver, whose prototype was integrated in a die with an area of 5 × 5 mm². Also, this receiver is fully compatible with commercial transmitters for the same frequency.

© 2011 Elsevier Ltd. All rights reserved.

1. Introduction

Invasive and implantable biomedical devices used for diagnosis and therapy, ranging from neural [1] to video-capsule endoscopy systems [2] are emerging innovative technologies and they are expected to originate significant business activity in the near future. The success of such systems is in part due to the advent of microtechnologies, which made possible the miniaturization of several sensors and actuators, as well their integration with readout and communication electronics. Wireless implantable microsystems constitute a breakthrough in the way the internal pathologies can be treated. This means that the radio-frequency (RF) chips can play an important role. In the context of implantable microsystems, the main contribution of this paper is the presentation of a super-regenerative receiver at 433 MHz. An important advantage inherent to this receiver is to be compatible with transmitters commercially available in the market. In this sequence of ideas, the target application for this receiver is in wireless microsystems for stimulating three nerves of the vertebral column, according to the desire of the patient, who presses a push-button to induce micturition and erection (in the case of males). The solution to send the electrostimulation commands can be a box containing a commercial off-the-shelf emitter module at 433 MHz using the same coding and modulation schemes of the receiver (e.g., codulation scheme [3]). The need for such transmission mode is because an RF chip solution is more suitable and reliable than the traditional approaches because the

latest solutions use wires for supplying the implantable devices and for transmitting data to these same devices [4].

2. Receiver design

2.1. The frequency of operation

The selection of a frequency for an implantable device is easy to do. First, the sizes of these devices must be as minimal as possible. In this context and as it is of general knowledge, the antenna is one of the most critical subsystems in wireless communications, which means that the antenna must be small enough to comply with size constraints of the microsystems to not compromise the desired miniaturization. The size reduction can be a problem because the antenna must be designed for transferring the highest possible power to the receiver. In the context of implantable devices, the size shortening of antennas can introduce additional problems of the impedance matching [7]. Additional issues include the biocompatibility and the bandwidth broadening for avoiding secondary effects related to frequency shifts. However, the environmental issue (and the most forgotten one) that limits the performance of an antenna (either transmitting or receiving antenna) is operating inside a lossy medium. This means that contrary to what happens in the free-space, the medium constituted by the human tissue will dominate the radiation performance of the whole RF link [8]. The antennas can be integrated with RF chips using either the on-package, or the on-chip or even the on-wafer technique. In case of on-package integration, the antenna is coupled into the package where the RF chip is supported. This first technique is the most simple of all. The on-chip integration requires more than one integration

process for more than one technology, which can lead to a situation where the technology for fabricating the RF chip can be incompatible with the one used for fabricating the antenna. Finally, the technique that seems to be promising is the on-wafer because wafer-level-packaging (WLP) techniques for joining heterogeneous technologies are offered by the industry with a relatively low-price. This last technique is especially suitable for integrating patch-antennas that are easy to package with the RF chips (due to their planar shape) [9]. A variety of antennas with a variety of shapes and physical placement are related in the literature, as it is in the work done by Soontornpipit et al. [10] who fabricated implantable patch antennas with spiral and serpentine shapes. The work from Mendes et al. [11] exploits the third dimension to fabricate small antennas with relatively good radiation characteristics. Finally, the research group of Chow et al. [12] explores an uncommon (but very innovative) methodology that makes profit of cardiovascular stents to receive RF signals inside the human body.

Previous works of biomedical applications at the frequency of 2.4 GHz [5], and the investigation of new frequencies [6] and new geometries [11] allowed the fabrication of small antennas to integrate in wireless microsystems [13,14]. This makes the selection of the most suitable frequency, one of the more decisive aspects in the design of RF transceivers. Normally, the desired range, baud-rate and power consumptions are key-aspects in the design to take into account for selecting the operation frequency. At a start-up point, the range limits the maximum usable frequency, because the loss suffered by the radiowaves in the free-space increases with the distance. The precise modeling of the propagation channel inside the human body in conjunction with the equation of skin-depth, δ (m), gives a rough estimation of the radiowaves penetration. The averaged parameters help to obtain the skin-depth and the path-loss characteristics of the propagation medium. However, the simple consideration of path-loss is not simpler because as stated by Scanlon et al. [15], the electrical parameters of the surrounding tissue around the RF receiver and the body's structure have a strong influence on the radiation pattern of the receiving antenna. The main consequences of this are difficulties due to fading caused by radiation pattern fragmentation especially observed in the azimuthal plane. This happens because the human body is composed by a variety of tissues comprising the skin, fat, muscle, bone, nerve, among others, it is required to do an averaging of the several electric parameters. A common role of thumb consists of applying a factor of 2/3 to the muscle, indicating that this is the dominating type of tissue in an average and healthy human subject [16]. It is a difficult task to obtain both the electric conductivity, σ (S m^{−1}), and the dielectric constant, ϵ_r , as the needed parameters for calculating the actual path-loss. Nevertheless and independent of the electrical parameters that are used, the following skin-depth equation can be used for obtaining an estimative of the expected path-loss [12,17]:

$$\delta = \left(2\pi 10^9 f_{\text{GHz}} \sqrt{\frac{\mu_0 \epsilon_0 \epsilon_r}{2} \left(\sqrt{1 + \left(\frac{18\sigma}{f_{\text{GHz}} \epsilon_r} \right)^2} - 1 \right)} \right)^{-1} \quad (\text{m}) \quad (1)$$

where $\epsilon_0 = 10^{-9}/(36\pi)$ F m^{−1}, $\mu_0 = 4\pi 10^{-7}$ H m^{−1}, are the electric permittivity and the magnetic permeability for the free-space (note that $(\epsilon_0 \mu_0)^{-1/2} = c$), respectively. The quantity f_{GHz} is the RF frequency expressed in giga-cycles per second.

To have an idea of how difficult it is to get the parameters, the cortical bone can present an electrical conductivity, σ , of 0.1032 S m^{−1} and a dielectric constant, ϵ_r , of 13.77 [16]. Additionally, in [18] these values are found to be $\epsilon_r = 5.2$, $\sigma = 0.11$ S m^{−1}, muscle $\epsilon_r = 57$, $\sigma = 1.12$ S m^{−1} and fat $\epsilon_r = 15$, $\sigma = 0.26$ S m^{−1} for bone, for

muscle and for fat, respectively. The difficulty is even more evident when looking at these parameters varying with frequency, as described in [16] where a disparity of values are presented: $\epsilon_r = 53$, $\sigma = 1.10$ S m^{−1} and $\epsilon_r = 51.6$, $\sigma = 1.56$ S m^{−1} for 418 and 916.5 MHz, respectively. This difficulty can also be used in a positive way, as it happened with the work done by Karacolak et al. [19] for continuously measuring the items of glucose (the variations of the electric parameters are used for measuring the sugar concentration). The previous parameters were used for obtaining the skin-depth for 433 MHz, 2.4 GHz and 5.7 GHz, whose values were observed to be much equal between them. This means that for high frequencies, the path-loss cannot be the only criterion to follow.

In the studies carried out by Siviak [20], the muscle tissue of the human body was modeled as a lossy wire antenna for simulating its interaction with radiowaves. More precisely, the human body was modeled as a cylinder of saline water with frequency dependent electrical parameters. These studies resulted in skin-depths of approximately 60 and 26 mm for 433 MHz and 2.4 GHz, respectively [20]. These statements help even more to support the use of 433 MHz with the less but still acceptable losses for implantable microsystems.

2.2. The super-regeneration principle

The super-regeneration principle was accidentally discovered by Edwin Armstrong in 1922 [21]. This principle is based on the switching between a stable and a (deliberated) non-stable status. Fig. 1(a) shows a simplified schematic of a super-regenerative receiver, where a resonant oscillator (whose oscillation frequency, f (Hz), is tuned to $f = (2\pi)^{-1}(LC)^{-1/2}$) can be seen. The produced resonances are maintained when the switch S is closed because current is supplied by an external electronic circuit (with a given transconductance, G_m (S)) to compensate the leakage current across the loss resistance, R_p (Ω) (due to the non-zero serial resistance of the inductance L and to the non-infinite parallel resistance of the capacitor C). As showed in Fig. 1(b), the current, I_x (A), is supplied by an external circuit and it must be such that $R_p = V_x/I_x$, thus the equivalent negative resistance, $R_{\text{neg}} = -R_p$ (for making $R_{\text{neg}}/R_p = \infty$) must be $R_{\text{neg}} = -1/G_m = -1/[I_x/V_x] = V_x/(-I_x)$. In fact, when the switch is closed, the receiver is operating in the logarithmic mode with the self-sustained oscillations being allowed to reach their maximum amplitude. In the situations when the switch is opened, the oscillations start to decay because there is no more injection of current to overcome the leakage in the loss resistance, R_p . The opening of the switch is an important task because the oscillations must be stopped (or extinguished) for restarting the super-regeneration process.

The clock signal in Fig. 1(a), V_{quench} (V), (with the period T_{quench} (t)) is called the quenching signal and it either opens or closes the switch S during $T_{\text{quench}}/2$ s in order to allow the oscillator to start the oscillations and to stop the oscillations. The oscillations envelope (that is limited by the supply voltage) increases exponentially after passing some instants of the switch closing. The time that lasts

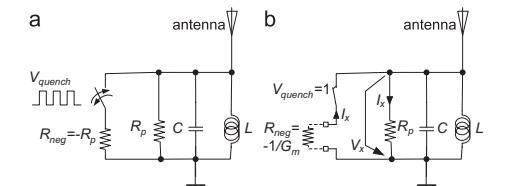


Fig. 1. (a) Simplified circuit of a super-regenerative receiver and (b) concept of negative resistance.

* Corresponding author.
E-mail address: jcarmo@dei.uminho.pt (J. Paulo Carmo).

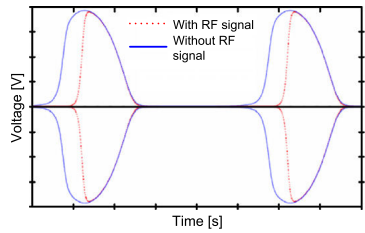


Fig. 2. Signal envelope in a super-regenerative receiver.

between the switch closing and the voltage increasing is dependent on the power of the RF signal in the antenna. Fig. 2 shows two situations of oscillations: with and without an RF signal in the antenna. As it can be observed, the oscillations start sooner in the presence of RF signals. The area enclosed by the envelope has a logarithmic relationship with the RF input power. Thus and since this operation mode is very sensitive to the RF power, it is possible to discriminate with great accuracy the presence or the absence of an OOK (on/off keying) modulated RF carrier. This operation mode is called super-regenerative and it requires the periodic extinction of the oscillations to discriminate the new presence or absence of the RF carrier in order to decode the new OOK symbol. This operation is done with the help of the quenching signal, which is internally generated by dividing the output of the counting circuit, e.g., the signal V_{count} .

2.3. A survey with the best and most recent state-of-the-art

The super-regenerative architecture allows the fabrication of receivers with high sensitivity and high simplicity of construction and low power consumption [22]. However, despite these positive points, this architecture was left forgotten for a long period of time due to inherent poor selectivity and frequency instability [23]. The interest in the super-regenerative receivers started to grow in the recent years with a tentative to make such receivers with commercial off-the-shelf components [24], culminating with a fully on-chip solution fabricated in a 0.8 μm BiCMOS process [25]. This last solution was one of the first successful approaches for obtaining integrated RF chips with receivers based on the super-regenerative architecture. Since these first steps were done, a wide variety of circuits were published in the literature for a wide number of applications fabricated with the available processes. The work done by Chen et al. [26] resulted in a receiver fabricated in a 0.13 μm CMOS process and able to operate at 2.4 GHz with passband tuning. The super-regenerative receiver fabricated by Moncuill-Geniz et al. [27] also operates at 2.4 GHz and was conceived for high-speed data transfer purposes (e.g., 11 Mbps). Finally, the work proposed by Moncuill-Geniz et al. [28] pushes the super-regenerative concept further by presenting two new architectures for achieving non-coherent detection of direct-sequence spread spectrum (DSSS) signals. To finish, it is expected that the potential for use the super-regenerative in modern applications did not reach the end-of-line and new developments are expected in the future.

2.4. The architecture of the receiver

Fig. 3 shows the block diagram of this super-regenerative receiver. As it can be observed, this super-regenerative receiver is composed by a resonant LC oscillator, two buffers, a quenching circuit and an envelope detector.

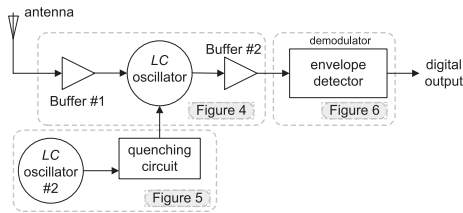


Fig. 3. Block diagram of the super-regenerative receiver at 433 MHz.

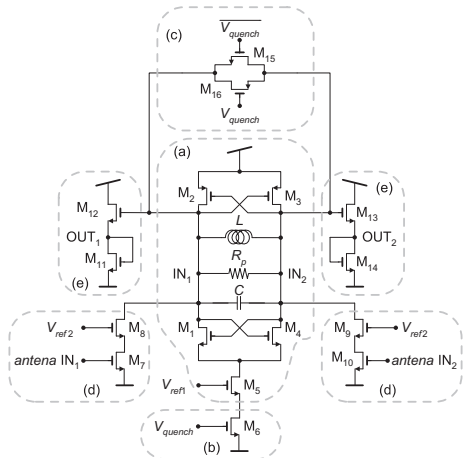


Fig. 4. Complete schematic of the front-end with the antenna, which comprises the following subsystems: (a) the LC oscillator that connects to the (b) quenching circuit; (c) the oscillations extinction circuit; (d) the backward to the antenna isolator (buffer number 1) and (e) buffer number 2 to isolate the LC oscillator and the subsequent circuits of the receiver.

As illustrated in Fig. 4(a), the selected topology for the LC oscillator was of complementary cross-coupled type with a dual pair of n- and p-type MOSFETs. The MOSFETs M_1 , M_2 , M_3 and M_4 provide the negative resistance effect, R_{neg} (Ω). The parallel pair of passive components composed by the capacitor C (F) and by the inductance L (H) provide the feedback between the two pairs of MOSFETs M_1/M_2 and M_3/M_4 . The condition to make the oscillations to grow must be such that the gain of the oscillator is $|G_m|R_{neg} = |G_m R_p| = |g_{m(n)} * g_{m(p)}| R_p \geq 2$. Apparently, the previous equation violated the Barkhausen criterion [29] and the statement formerly presented (e.g., $R_{neg} = -1/G_m$), but this is while the oscillations are growing until the saturation and the MOSFETs start to operate in the saturation region. Thus, the Barkhausen criterion will apply in this situation and $|G_m|R_{neg} = 1$.

The MOSFET M_5 uses the reference voltage $V_{ref1} = 0.93$ V to limit the bias current to 10 μA , while the MOSFET M_6 (a part of the quenching circuit) is controlled by the signal V_{quench} to switch on and off the LC oscillator. The passive components of the LC oscillator are selected to have a resonant frequency of 433 MHz. The part (c) of the circuit in Fig. 4 (the antenna front-end) is a transmission gate (synchronized with the quenching signal) to

short-cut the two output terminals of the LC oscillator during its disabling, thus decreasing the extinction time of the oscillations. The part (d) of the antenna front-end is a cascade current source and it is used to couple the RF signal from the antenna to the LC oscillator. Thanks to its cascade topology, the backward isolation is high, thus the coupling of the oscillatory signals into the antenna is low. In this sequence of ideas, the receiver contains an output buffer (buffer number 2 in Fig. 3 and in Fig. 4(e)) to isolate the LC oscillator from the rest of the receiver in order to minimize the load effect and to not interfere with the correct operation of the oscillator (e.g., minimizing the contribution for the phase and frequency noise in the generated oscillations). The buffer number 2 uses a differential source follower, whose gain (that is less than unity) was selected to minimize the attenuation of the oscillatory signal and is $A_v = [1 + (W_{14}/L_{14})^{1/2} (W_{13}/L_{13})^{-1/2}]^{-1} = 0.8$.

As it was said before, the quenching circuit supervises the super-regeneration process and at the same time it provides a synchronized control signal to short-circuit the outputs of the LC oscillator, which in the meanwhile was switched off, thus decreasing the time of oscillatory signal extinction. Fig. 5 shows both (a) oscillator number 2 of Fig. 3 and (b) the quenching signal generator. The second oscillator is a Pierce piezoelectric-type oscillator and uses a piezoelectric crystal (with a high quality factor) to generate a stable signal for controlling the quenching switch. The quenching signal is obtained from a signal with a frequency of 4 MHz after a division by eight, resulting in a signal with a frequency of 500 kHz.

A differential topology was selected for implementing the LC oscillator due to its improved noise immunity, thus a differential-to-single-ended conversion circuit is needed to connect this

oscillator to the envelope detector. As is it is illustrated in Fig. 6, such a purpose is achieved with a differential amplifier (with the OUT_1/OUT_2 inputs and the V_{single} output). The voltages at the inputs of the differential amplifier are $V_1 = V_{CM} + V_{RF}(t)$ and $V_2 = V_{CM} - V_{RF}(t)$, whose common mode voltage, V_{CM} (V), must be high, thus the coupling of the oscillatory signals into the antenna is low, thus the coupling of the oscillatory signals into the antenna is low.

The single-ended RF signal is converted to a sequence of pulses after passing the envelope detector and the level adjusting circuit. As it can be observed in Fig. 6(b), the capacitor C (F) filters the single-ended signal to remove the abrupt variations. The created effect is similar to envelope detection. However, the amplitude of the signal V_{single} (V) is low and must be amplified. This is done with a common source topology constituted by the resistor R_4 (Ω) and by the n-MOSFET M_{27} . The two further inverters (constituted by the MOSFETs M_{28} – M_{31}) create a digital signal from the filtered single-ended voltage, V_{single} . The demodulated signal, $V_{demodulated}$ (V), has a pulsed shape in the presence of RF signals at the antenna and its frequency is the same as the quenching signal, $V_{quenching}$. The output signal is null without RF signals, thus for this reason it is necessary to use a variation of the Manchester code for sending an information bitstream.

3. Results

Fig. 7 shows several signals inside the receiver in a response to an RF signal with an amplitude of 100 μV . It is important to note that the differential signal given by the single-ended signal obtained from the difference $OUT_1 - OUT_2$ is correctly filtered, thus the envelope detection is correctly done. The amplified

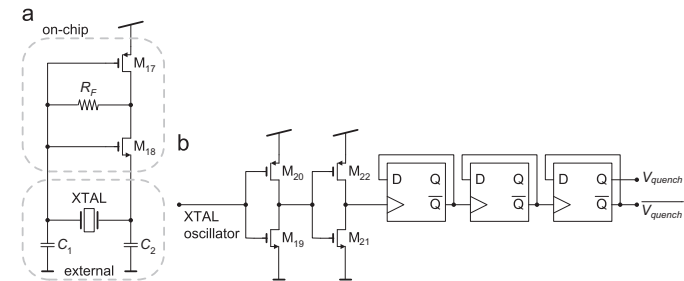


Fig. 5. Electronic schematic of the (a) oscillator number 2 and (b) quenching circuit.

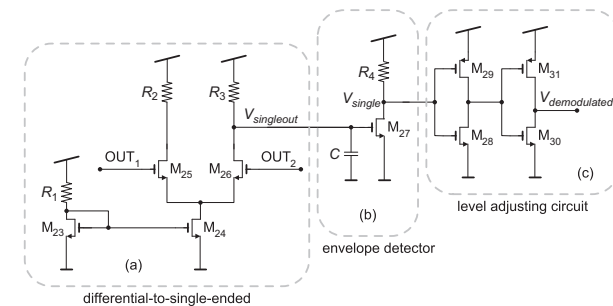


Fig. 6. Electronic circuit of the demodulator, which is composed by (a) a differential-to-single-ended converter, (b) an envelope detector and (c) a level adjusting circuit.

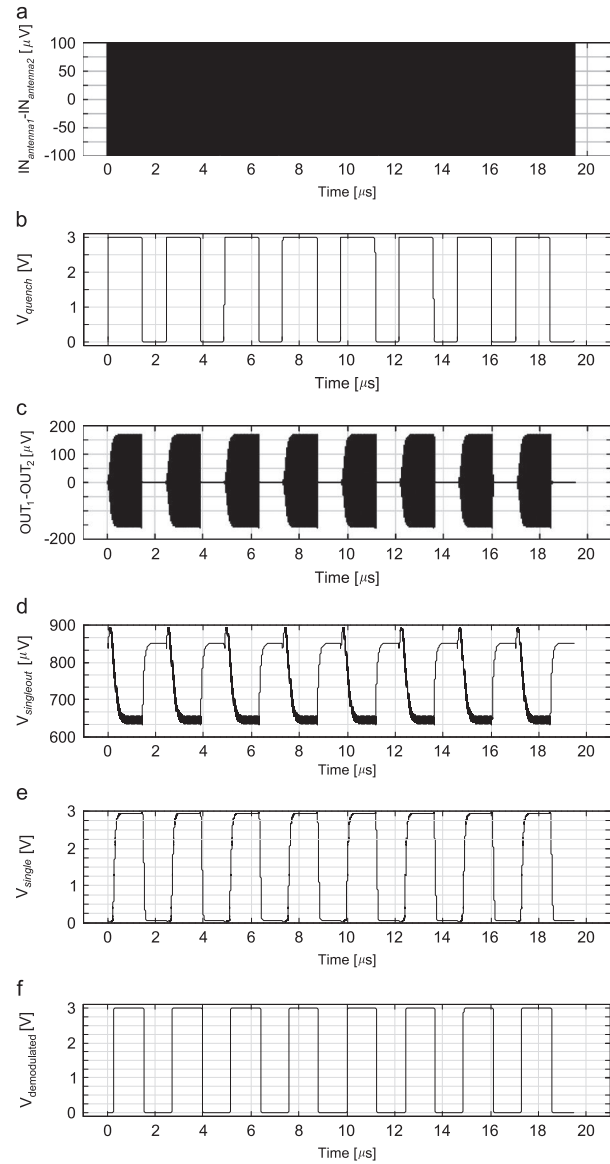


Fig. 7. Simulations showing (a) differential RF signal at the antenna, antenna IN₁–antenna IN₂ (µV), (b) quenching signal, V_{quench} (V), (c) differential signal at the output of the LC oscillator, OUT₁–OUT₂ (µV), (d) filtered version of the signal at the end of the differential-to-single-ended converter, V_{singleout} (µV), (e) amplified version of the single-ended signal, V_{singleout} (V) and (f) pulsed signal at the output of the receiver, V_{out} (V).

version, V_{singleout} (V), of the single-ended signal is then obtained and gives rise to a pulsed signal in the receiver (which further in conjunction with a coding scheme will allow the discrimination of the received binary symbol, e.g., the received bit).

As shown in Fig. 8(b), this receiver was designed for transmitting binary data modulated in OOK coded with a modified version of the Manchester code (e.g., a kind of Biphase code). The carrier is injected during the first 80% of the bit duration for transmitting a “0”. In the opposite situation, a “0” is transmitted when the carrier is injected during 20% of the bit duration after its suppression on the initial 80% of bit duration. Fig. 8(c) shows the pulse-shaped signal at the output of the receiver, where the possibility to discriminate the received bitstream without ambiguities can be observed.

During the simulations, the amplitude of a differential RF unmodulated signal, antenna IN₁ – antenna IN₂ (V), (e.g., a continuous 433 MHz carrier) was varied between 0 V and 200 mV. The receiver responded correctly with a pulsed signal output – see Fig. 8(c) – for RF signals with amplitudes, A_{RF} (V), between

100 µV and 100 mV. This amplitude range can be used to obtain the power range of operation:

$$P_{in} = 10 \log_{10} \left(\frac{A_{RF}^2}{100} \right) = -20 + 20 \log_{10}(A_{RF})(dB) \quad (2)$$

The calculation of RF power signal is done in a straightforward form, resulting in the [–100, –40] dB range. This large dynamic range has potential for implantation in humans because the receiver is tolerant to amplitude fluctuations in the RF signal.

As shown in Fig. 8, the signal at the output of the receiver presents a pulsed shape with a frequency equal to those in the quenching signal. The 20%/80% modified version of the Manchester coding imposes the existence of at least one or four pulses at the output when either a “1” or a “0” is transmitted, thus the maximum baud-rate, R_b (bps), must be equal to one fifth part of the quenching frequency, f_{quenching} (Hz), which for the illustrated case is R_b = 20000/5 = 4 Kbps. Moreover, the quenching signal can be used for clock synchronization purposes in further base-band circuits without the need to use additional circuits for doing such a task.

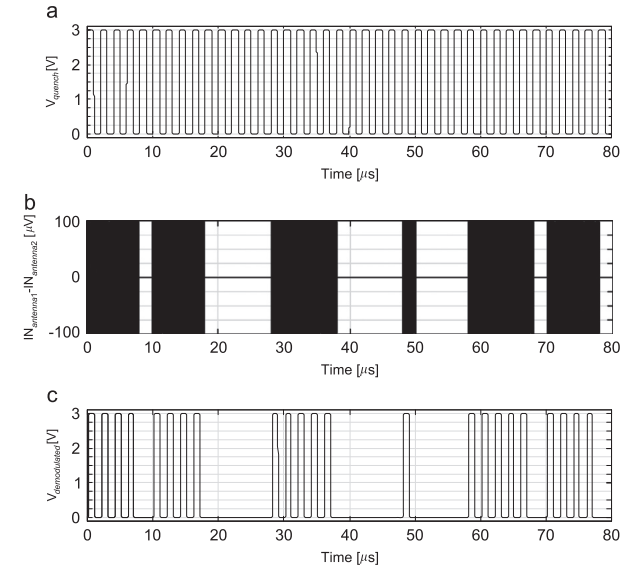


Fig. 8. Simulations showing (a) quenching signal, V_{quench} (V) at 500 KHz, (b) differential RF signal at the antenna IN₁–IN₂ (V) and (c) signal at the pulsed output of the receiver, V_{out} (V).

Table 1
Comparison of RF receivers found in the best state-of-the-art with the one presented in this paper.

Receiver	Frequency (GHz)	Technology	Sensitivity (dBm)	Power consumption (mW)	Voltage (V)	Modulation and coding
This paper	0.433	0.7 µm	–70	4.4	3	OOK and Biphase
[21]	1	0.35 µm	–107	1.2	1.4–3	
[22]	1	0.8 µm	–105	3.6	2.4	OOK
[25]	1	BiCMOS	–98	1.2	2	
[26]	2.4	0.13 µm	–90	2.8	1.2	
[27]	2.45	Bipolar	–81	1.75	1.2	OOK (Gaussian bit envelope)
[28]	2.4		–90	350	5	OOK and DSSS

This will result in an additional power saving, which is a non-negligible item in the context of implantable devices. Table 1 compares this RF receiver with the best super-regenerative state-of-the-art found in the literature. It is possible to observe in Table 1 that the proposed receiver offers a good compromise between power consumption and supply voltage. Moreover, the 433 MHz frequency is more appropriate for use in implantable devices because as previously stated, e.g., it is less sensitive for propagation into the human body (which is lossy and not homogeneous). The receiver was fabricated taking into account the emphasis on low-cost and repeatability. For achieving such goals, the 0.7 μm CMOS process seems to be a good choice because it is available worldwide at low price and well established (e.g., matured and trimmed from their electronics characteristics and parameters spreading points of view).

4. Conclusions

This paper presented a super-regenerative receiver at 433 MHz for use in wireless implantable microsystems. The frequency of 433 MHz was selected because it allows the reception of RF signals inside the human body. The receiver can be supplied with a voltage of 3 V and allows the reception of RF signals with powers in the range of $[-100, -40]$ dB. The modulation scheme is based on the on/off keying amplitude (OOK) modulation plus a modified version of the Manchester code (a Biphase code). Despite the simplicity of the OOK modulation, this receiver is compatible with commercial RF transmitters (naturally, working with the same carrier frequency). The use of OOK modulation allows the design of a future transmitter where the carrier can simply be switched on and off, and thus the frequency synthesizer circuit can be relaxed [30]. Fig. 9 shows a photograph of the first prototype of the fabricated receiver (the red area), which was fabricated in the AMIS 0.7 μm CMOS process.

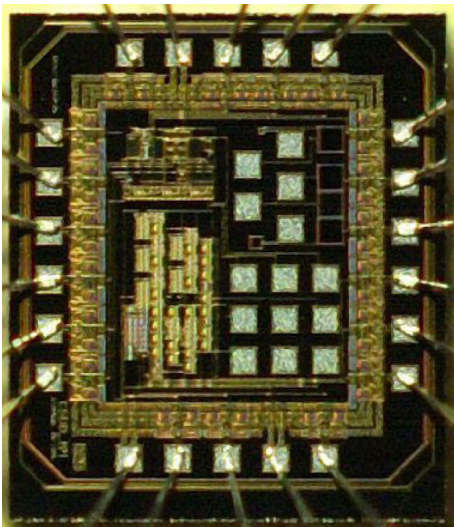


Fig. 9. A die photograph of the first prototype of the super-regenerative receiver (1.6 mm \times 1.5 mm size dimensions). (For interpretation of the references to color in this figure legend, the reader is referred to the web version of this article.)

References

- [1] K.T. Lau, S.T. Lee, P.K. Chan, A low-power synapse/neuron cell for artificial neural networks, *Microelectronics Journal* 30 (1999) 1261–1264.
- [2] B. Chi, J. Yao, S. Han, X. Xie, G. Li, Z. Wang, Low power high data rate wireless endoscopy transceiver, *Microelectronics Journal* 38 (2007) 1070–1081.
- [3] B. Pattan, *Robust Modulation Methods and Smart Antennas in Wireless Communications*, Prentice Hall, 1999.
- [4] J. Sacristán-Riquelme, M.T. Osés, Implantable stimulator and recording device for artificial prosthesis control, *Microelectronics Journal* 38 (2007) 1135–1149.
- [5] J.P. Carmo, P.M. Mendes, C. Couto, J.H. Correia, A 2.4 GHz low-power/low-voltage wireless plug-and-play module for EEG applications, *IEEE Sensors Journal* 7 (11) (2007) 1524–1531 full paper in Acrobat PDF, November.
- [6] P.M. Mendes, J.H. Correia, M. Bartek, J.N. Burghartz, Analysis of chip-size antennas on lossy substrates for short-range wireless microsystems, in: Proceedings of the SAFE 2002, 51–54, Veldhoven, The Netherlands, November 2002.
- [7] M.D. Weiss, J.L. Smith, J. Bach, RF coupling in a 433 MHz biotelemetry system for an artificial hip, *IEEE Antennas and Wireless Propagation Letters* 8 (2009) 916–919.
- [8] A.K. Skrivervik, F. Merli, On the efficient design, analysis and measurement of bio-compatible electrically small antennas, in: Proceedings of the 2010 URSI International Symposium on Electromagnetic Theory, Berlin, Germany, August 2010, pp. 853–856.
- [9] A. Polyakov, S. Sinaga, P.M. Mendes, M. Bartek, J.H. Correia, J.N. Burghartz, High-resistivity polycrystalline silicon as RF substrate in wafer-level packaging, *Electronic Letters: The IET* 41 (2) (2005) 100–101.
- [10] P. Soontornpipit, C.M. Furse, Y.C. Chung, Design of implantable microstrip antenna for communication with medical implants, *IEEE Transactions on Microwave Theory and Techniques* 52 (8) (2004) 1944–1951.
- [11] P.M. Mendes, A. Polyakov, M. Bartek, J.N. Burghartz, J.H. Correia, Integrated chip-size antennas for wireless microsystems: Fabrication and design considerations, *Journal of Sensors and Actuators—A* 125 (2006) 217–222.
- [12] E.Y. Chow, Y. Ouyang, B. Beier, W.J. Chappell, P.P. Irazoqui, Evaluation of cardiovascular stents as antennas for implantable wireless applications, *IEEE Transactions on Microwave Theory and Techniques* 57 (10) .
- [13] F. Touati, M. Pons, On-chip integration of dipole antenna and VCO using standard BiCMOS technology for 10 GHz applications, in: Proceedings of the 29th ESSCIRC, Estoril, Portugal, September 2003, pp. 493–496.
- [14] J.P. Carmo, P.M. Mendes, C. Couto, J.H. Correia, 5.7 GHz on-chip antenna/RF CMOS transceiver for wireless sensors, *Journal of Sensors and Actuators—A* 132 (1) (2006) 47–51 Science Direct.
- [15] W.G. Scanlon, J.B. Burns, N.E. Evans, Radiowave propagation from a tissue-implanted source at 418 MHz and 916.5 MHz, *IEEE Transactions on Biomedical Engineering* 47 (4) (2000) 527–534.
- [16] D.A. Christensen, C. Furse, C.H. Durney, D.A. Christensen, *Basic Introduction to Bioelectromagnetics*, second ed., CRC Press, 2009.
- [17] J.L. Volakis, *Antenna Engineering Handbook*, fourth ed., McGraw-Hill Professional, 2007.
- [18] R. Pethig, Dielectric properties of body tissues, *Clinical Physics and Physiological Measurement: Institute of Physics (IOP)* 8 (Suppl. A) (1987) 5–12.
- [19] T. Karacolak, A.Z. Hood, E. Topsakal, Design of a dual-band implantable antenna and development of skin mimicking gels for continuous glucose monitoring, *IEEE Transactions on Microwave Theory and Techniques* 54 (4) (2008) 1001–1008.
- [20] K. Siwiak, *Radiowave Propagation and Antennas for Personal Communications*, third ed., Artech-House, 2007.
- [21] A. Vouilloz, M. Declercq, C. Dehollain, A low-power CMOS super-regenerative receiver at 1 GHz, *IEEE Journal of Solid-State Circuits* 36 (3) (2001) 440–451.
- [22] N. Joehl, C. Dehollain, P. Favre, P. Deval, M. Declercq, A low-power 1 GHz super-regenerative transceiver with time-shared PLL control, *IEEE Journal of Solid-State Circuits* 36 (7) (2001) 1025–1031.
- [23] D.M.W. Leenaerts, Chaotic behavior in super regenerative detectors, *IEEE Transactions on Circuits and Systems I: Fundamental Theory and Applications* 43 (3) (1996) 169–176.
- [24] D.L. Ash, A low-cost super-regenerative SAW stabilized receiver, *IEEE Transaction on Consumer Electronics* 33 (1987) 395–404.
- [25] P. Favre, Member, N. Joehl, A. Vouilloz, P. Deval, C. Dehollain, M.J. Declercq, A 2 V 600 μA 1 GHz BiCMOS super-regenerative receiver for ISM applications, *IEEE Journal of Solid-State Circuits* 33 (12) (1998) 2186–2196.
- [26] J.-Y. Chen, M.P. Flynn, J.P. Hayes, A fully integrated auto-calibrated super-regenerative receiver in 0.13 μm CMOS, *IEEE Journal of Solid-State Circuits* 42 (9) (2007) 1976–1985.
- [27] F.X. Moncunill-Geniz, P. Palà-Schönwälder, C. Dehollain, N. Joehl, M. Declercq, An 11 Mb/s 2.1 mW synchronous super-regenerative receiver at 2.4 GHz, *IEEE Transactions on Microwave Theory and Techniques* 55 (6) (2007) 1355–1362.
- [28] F.X. Moncunill-Geniz, P. Palà-Schönwälder, F. del Águila-López, New super-regenerative architectures for direct-sequence spread-spectrum communications, *IEEE Transactions on Circuits and Systems II: Express Briefs* 52 (7) (2005) 415–419.
- [29] B. Razavi, *RF Microelectronics*, Prentice Hall, 1997.
- [30] R. Morais, A. Valente, C. Couto, J.H. Correia, A wireless RF CMOS mixed-signal interface for soil moisture measurements, *Journal of Sensors and Actuators—A* 115 (2004) 376–384.